Optics Communications 336 (2015) 255–261

Contents lists available at ScienceDirect

Optics Communications

journal homepage: www.elsevier.com/locate/optcom

Digital holographic microscopy for microalgae biovolume assessment

Andrea C. Monaldi*, Gladis G. Romero, Elvio E. Alanís, Carlos M. Cabrera

Universidad Nacional de Salta, Grupo de Óptica Láser, Facultad de Ciencias Exactas INENCO-CONICET, Argentina

ARTICLE INFO

Article history:
Received 15 April 2014
Received in revised form
6 October 2014
Accepted 12 October 2014
Available online 18 October 2014

Keywords:
Digital holographic microscopy
Biovolume
Microalgae
Image processing
Phytoplankton refractive index
Ceratium Hirundinella

ABSTRACT

The relative amount of biomass in a body of water is one of the various indicators widely used in water quality evaluation. This implies complex tasks such as identification and characterization of microorganisms and measurement of their biovolume. Particularly, the latter is estimated by assuming simple geometrical shapes for the microorganism and by calculating its dimensions from images taken with a conventional microscope. In order to have a more precise and automatic method for biovolume evaluation, a hybrid methodology based on digital holographic microscopy and image processing is proposed. The whole volume of a specimen under study is obtained combining the phase contrast image of an off-axis hologram with the thickness-profile data of the specimen extracted from the cell silhouette. This technique has been used for determining the biovolume of *Ceratium Hirundinella* cells in water samples. The methodology proposed also shows that it is possible to estimate accurately an *effective refractive index* of the microorganism. Experimental results have shown that this technique is not only an efficient and fast alternative, but also suitable for automatizing the entire process.

1. Introduction

In Biology and Medicine, identification, quantification, characterization and detection of microorganisms such as parasites, bacteria, and microalgae, are particularly important as diagnosis tools [1–6]. Generally, these observations are carried out under a microscope by highly specialized technicians. Many times, the morphology of these specimens is complex and the performance of the analysis strongly depends on its correct identification and quantification, which is a tiring and time-consuming task. Particularly, the estimation of microalgae biovolume is one of the most widely studied morphometric descriptors and it is important for the study of phytoplankton ecology. Related parameters, such as cell size, carbon content and physiology functions are also important for marine ecosystem studies. This calculation is performed by associating microalgae with simple geometrical shapes and by determining their volume measuring linear dimensions with an ordinary microscope [7–10]. Briefly, this procedure consists of measuring at least twenty individual cell biovolume for each of the species. After that, the average biovolume is multiplied by the number of cells/ml in order to obtain its relative abundance. In addition, this complex methodology contributes with approximate values only.

In the last decades, taking advantage of digital cameras equipped with CCD or CMOS sensors, and digital image processing tools, holography field has gained new interest due to the so-called digital holography (DH) [11]. Since 1999, digital holographic microscopy (DHM) has emerged as an interesting alternative to conventional microscopy [12–16]. A digital hologram, consisting of the interference between an object and a reference beam, is recorded by a digital camera and the holographic image is numerically reconstructed using diffraction theory basis. Calculation of the complex optical field allows direct access to quantitative amplitude and phase information [10]. Moreover, numerical focusing is possible by reconstructing the single recorded hologram at several distances, emulating the focusing control of a conventional microscope. In all these approaches, the phase signal provided by DHM is obtained using a transmission configuration and it is proportional to the integrated optical path length (OPL) along the optical axis through the specimen, depending on both, morphology and mean intracellular refractive index. Although methods to decouple both variables exist [13], the measurement remains as an integrated value. Recently, multiple angles digital holographic tomography and tomographic phase microscopy have rapidly evolved to recover a full three-dimensional (3D) refractive index map of intracellular structures, or to estimate the three-dimensional morphology and shape of microsamples. Nevertheless, these techniques rely on some mechanical scanning achieved either by rotating the object [15,17,18] or varying the illumination

* Correspondence to: Universidad Nacional de Salta, Fac. de Cs. Exactas, Av. Bolivia 5150-4400 Salta, Argentina. Tel.: +54 387 4255581.
E-mail address: acmonaldi@gmail.com (A.C. Monaldi).

http://dx.doi.org/10.1016/j.optcom.2014.10.035
0030-4018/

beam angle [19], or involve the use of continuous tunable laser [20,21].

In the present paper, we propose a simple methodology that combines the information obtained from only two holograms with image processing tools, to determine biovolume of *Ceratium Hirundinella*. These microalgae are dominant members of the summer phytoplankton and can develop algal blooms as a result of cell rapid growth. As a consequence, they affect the ecosystem of water bodies causing mass mortalities in fish and taste and odor problems in drinking water. These events have occurred recently in Argentina, dating just from the last two decades, thus the interest in studying this species has increased. In addition, it is important to emphasize the fact that it is not only important to estimate the number of microorganisms in a sample, but also to devote more attention to the estimation of biovolume and biomass of individual species [10]. In this sense, because of *C. Hirundinella* large size, they might actually contribute a major fraction of the overall biomass in mixed-species samples.

The present study is performed in water samples containing *C. Hirundinella* collected from the La Cienega dam, Jujuy Province, Argentina. *C. Hirundinella,* are dinoflagellates microorganisms of 80–400 μm in length. They are strongly compressed dorsoventrally, they have an apical long and narrow horn with a blunt tip and antapical horns straight with pointed closed tips. The antapical horns are normally slightly diverged from each other distally; they also present an excavation in the ventral side, providing an additional geometrical complexity. The quite variable shape of the cell requires complicated equations for the biovolume calculations by geometrical approximations, demanding several lengths and diameters measurements per cell [8]. These properties are evidenced out in the photograph of a conventional microscope field in Fig. 1, taken with a 10 × Microscope Objective (MO). Moreover, a certain degree of uniformity of cell size distribution is observed. As it can be seen in Fig. 1, the largest number of *C. Hirundinella* cells in a sample lie on frontal position, while some others lie in dorsoventral position, as shown in the highlighted area of the same figure.

Taking advantage of this fact and of the size uniformity, the calculation of biovolume is performed using a single hologram of the specimen at each of these positions. From holograms of the cell in frontal position, phase delay introduced is obtained. This information is combined with an average cell thickness extracted from the silhouette measured from holograms of the individuals that appear in dorsoventral position. The calculation, which does not require any sophisticated devices, is part of an automated system for determination of the relative abundance of microorganisms in water samples, whose main aim is to provide a portable tool that can be used by specialist on the sampling site to perform biovolume measurements *"in situ"*.

Fig. 1. A typical field of view of a water sample containing *C. Hirundinella*, taken with a conventional microscope.

2. Instruments and methods

2.1. Holograms registration and reconstruction

The transmission DHM and phase image reconstruction techniques used for the present study have been described in Refs. [11,12,21]. Briefly, they consist of recording a hologram by means of an interferometric set-up, onto a solid state array detector such as a CCD or CMOS sensor and, subsequently, numerically reconstructing the information by means of a computer. A layout of DH Microscope prototype constructed for this purpose, is depicted in Fig. 2(a).

Essentially, it is a Mach–Zehnder interferometer, whose object arm is fitted with a small microscope built by inserting an *X*–*Y* microscope stage to put the sample and a microscope objective (MO) which acts as a magnifying lens and forms a real image of the specimen, as it is illustrated in Fig. 2(b). To facilitate the automatic search of a field containing microalgae, the plate of the DH microscope is driven by two step motors to orderly scan consecutive fields of view.

The most remarkable feature of this architecture, early proposed by Van Ligten and Osterberg [22], is that the hologram plane (sensor plane) is located between the MO and the image plane at a distance *d* from the latter. This is equivalent to a holographic arrangement without lenses, with an object wave emanating directly from the magnified image instead of the object itself. Therefore, the hologram consists of an unfocused image of the sample modulated by the interference fringes formed by the object and the reference beams, as shown in Fig. 3(a). The polarized collimated light beam originated at a He–Ne laser of wavelength $\lambda = 632.8$ nm is divided by a beam splitter BS_1 in order to obtain the object and the reference beams. The plane wave that travels through the object arm, after being reflected by the mirror M_1, illuminates the sample to be analyzed. The wave diffracted by the specimen, is collected and magnified by a 20 × /0.40 NA or a 10 × / 0.25 NA objective, MO_1. At the same time, the plane wave that travels through the reference arm is reflected by the mirror M_2, and magnified by MO_2, with the same characteristics of MO_1, to match the curvatures of the two wave fronts. The object beam and reference beam are recombined in the second beam splitter, BS_2, and interfere at the output of the interferometer. A TV camera, with a CMOS Bayer Array 2592 × 1944 pix^2, 1.75 μm square pixels, 8 bit deep and a frame rate up to 25 Hz is used to record this interference pattern (digital holograms). A grabbed frame of this sequence cropped at 512 × 512 pix^2 size is temporarily stored in the buffer of an image digitizer board for further processing.

The reconstruction of the original microscopic field of view of the sample is performed digitally on a computer. This procedure simulates the reconstruction process in conventional holography, which consists of illuminating the hologram with a replica of the reference beam *R* used in the registration stage. Literature describes several methods to retrieve the complete information of the object wave in both, amplitude and phase [11,12]. In this application, the reconstruction of holograms is carried out by using the angular spectrum propagation method. The reconstructed wave front, both in amplitude and phase, are shown in Fig. 3 (b) and (c) respectively. The latter is a two-dimensional phase distribution called the wrapped phase image. Since this wrapped phase suffers from 2-π phase jumps, it is unusable until the phase discontinuities are removed. Therefore, a procedure of phase unwrapping must be performed in order to recover the true continuous phase values to denote real physical quantity. Many phase unwrapping algorithms have been developed during the last three decades [23–27]. In this application, the quality guide phase unwrapping algorithm [27], is used to retrieve the continuous phase

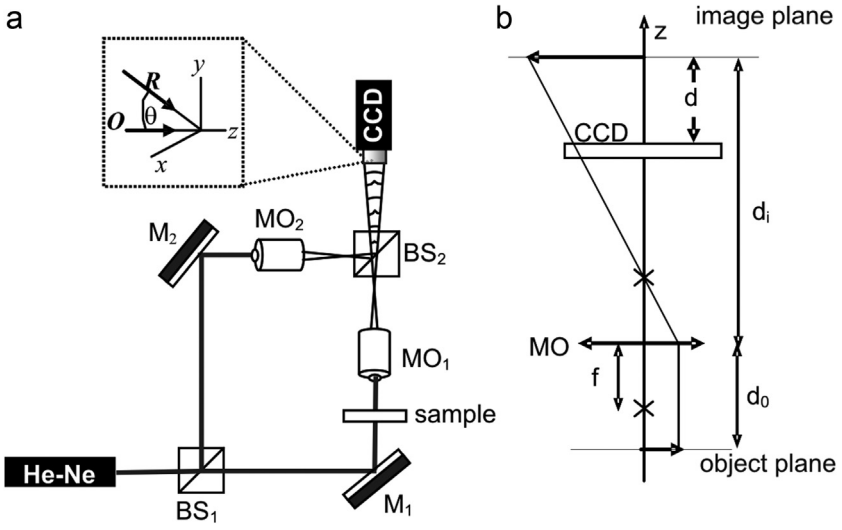

Fig. 2. (a) Experimental configuration; BS, beam splitters; M, mirrors; MO, microscope objectives. Inset: R, reference beam; O, object beam. (b) Details of the microscope configuration in the object arm: d_0, object distance; d_i, image distance; f, MO focal length; d, distance of the image relative to the CCD sensor.

map. In Fig. 3(d) and (e) the unwrapped phase contrast image and its 3D perspective representation are shown.

2.2. Biovolume estimation

Biovolume determination is obtained from the continuous phase maps of the microalgae. Considering Fig. 3(d), for an arbitrary pixel *(i, j)* within the cell, the total phase delay experienced by the light signal through the sample in the z direction perpendicular to the hologram plane, is given by:

$$\phi(i,j) = \frac{2\pi}{\lambda}\left[n(i,j)h(i,j) + n_0(D - h(i,j)) + n_g t\right] \quad (1)$$

where $n(i,j) = 1/h(i,j)\int_0^{h(i,j)} n_{c,ij}(z)\,dz$ is the integral value of the intracellular refractive index $n_{c,ij}$ along the specimen thickness $h(i,j)$; n_0 is the constant refractive index of the surrounding medium;$n_g$is the constant glass refractive index; t the thickness of the slide and coverslip overall, and D is the total height of the sample.

Assuming that the surrounding medium refractive index and the slide-coverslip refractive index are approximately constant, phase signal contributions introduced by them can be easily avoided by subtracting the median value of the total phase signal. By rearranging Eq. (1), it is easy to show that for each pixel (i, j) the component of the phase signal, which is specific to the cell, is

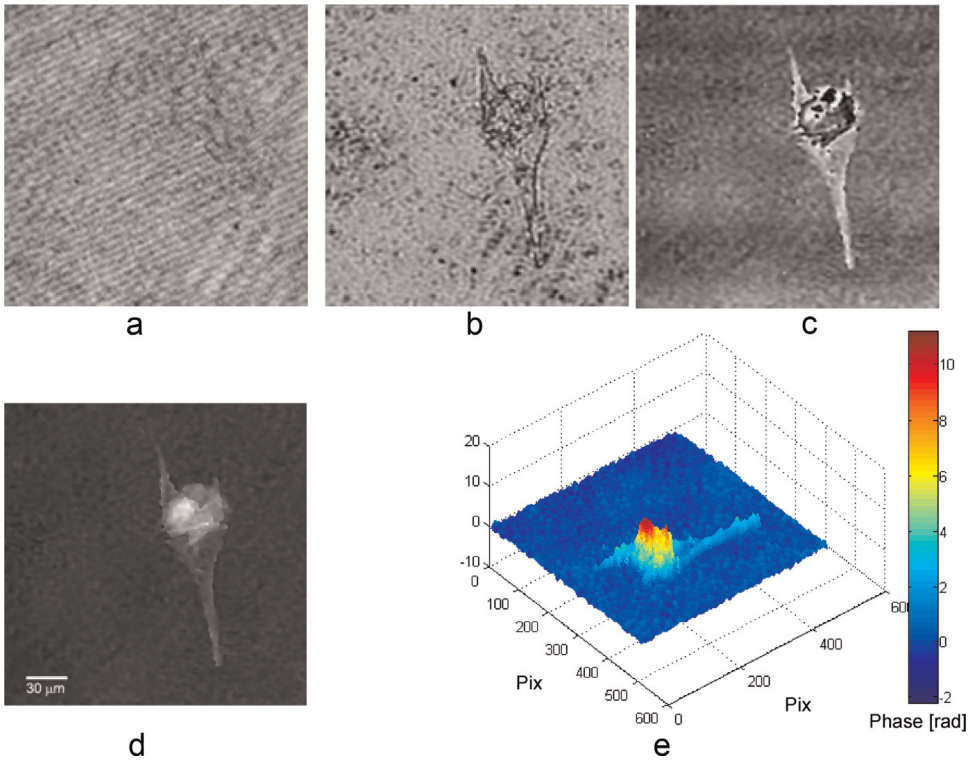

Fig. 3. (a) Hologram of a *C. Hirundinella*, (b) amplitude contrast image, (c) wrapped phase contrast image, (d) unwrapped phase image, and (e) 3D perspective representation of (d).

given by:

$$\phi(i,j) = \frac{2\pi}{\lambda}(n(i,j) - n_0)h(i,j) = \frac{2\pi}{\lambda}\Delta n(i,j)h(i,j) \quad (2)$$

This equation shows that the phase lag introduced by the cell at each point, depends on both, the cell thickness, required for calculation of algal biovolume, and the difference between the intracellular refractive index and the surrounding media refractive index. Moreover, these quantities are coupled; in this sense, regions of the cell with identical thickness may introduce very different phase delays; for example, regions in which the nucleus is located might have the highest refractive index and therefore make the major contribution the phase delay. Thus, for determining algal biovolume from the phase information given by Eq. (2), it is necessary to know $n(i,j)$ values, for each pixel within the specimen. Unfortunately, phytoplankton is quite heterogeneous, and generally sophisticated techniques are required to measure integral refractive index [13]. Instead, it is possible to know the average phytoplankton refractive index by flow cytometric tehchniques and Mie theory [28], or by theoretical estimations according to its metabolite composition [29]. In the case of the latter; for phytoplakton in sea water, refractive index values at 589 nm ranged from 1.366 to 1.473, with a mean value of 1.419 are accepted depending on algal water content.

Since the biovolume is a global quantity, assuming an average refractive index is attractive because it gives a meaningful value for a variety of microalgae classes, even though the heterogeneity of intracellular content. However, as an underlying assumption, it implies an identical internal structure of each cell under study, and it does not take into account large differences in intracellular content, either between different species or within the same species. Therefore, in this paper we propose to estimate an *effective refractive index* $\bar{n}$ for each cell under study in order to determine its individual biovolume. Although this assumption does not allow to obtain the exact value of each $h(i,j)$, the calculated value using an effective refractive index would be equally representative. From Eq. (2), it follows that the cell equivalent thickness in each point is given by:

$$h^*(i,j) = \frac{\lambda}{2\pi}\frac{\phi(i,j)}{\Delta\bar{n}} \quad (3)$$

being $h^*(i,j)$ an equivalent thickness for the (i,j) pixel, assuming that the refractive index of the entire cell is uniform, so that $\Delta\bar{n} = \bar{n} - n_0$ is constant. This conjecture also implies that higher phase delays are tied to higher equivalent thickness without affecting the biovolume estimation accuracy, as it will be discussed in the next section.

Algal biovolume is then calculated by adding all elementary volumes $h^*(i,j)\Delta x\Delta y$:

$$V = \sum h^*(i,j)\Delta x\Delta y = \sum \frac{\lambda}{2\pi}\frac{\phi(i,j)}{\Delta\bar{n}}\Delta x\Delta y \quad (4)$$

where Δx and Δy are the pixel size in the image according to the magnification of the microscope objective used.

As explained in Section 1, *C. Hirundinella* are strongly compressed dorsoventrally, thus it is more usual to find them in frontal position; nonetheless, occasionally they can be observed in dorsoventral position. Hence, exploiting this feature, a method for estimating $\Delta\bar{n}$ for each cell is proposed. This method consists of combining information data extracted from two microalgae positions, dorsoventral and frontal respectively.

From the former, it is possible to extract the silhouette which gives the maximum thickness values of the hidden dimension of the cell in Fig. 3(d). This task is accomplished recording a hologram of the cell in dorsoventral position and then reconstructing it for extracting the region-of-interest (ROI) from the phase contrast maps, as shown in Fig. 4(a). For this purpose, the phase image is first rotated until the cell is layed down and then binarized, in order to obtain the silhouette of the cell, as shown in Fig. 4(b) and (c) respectively. All these steps are carried out by automated image

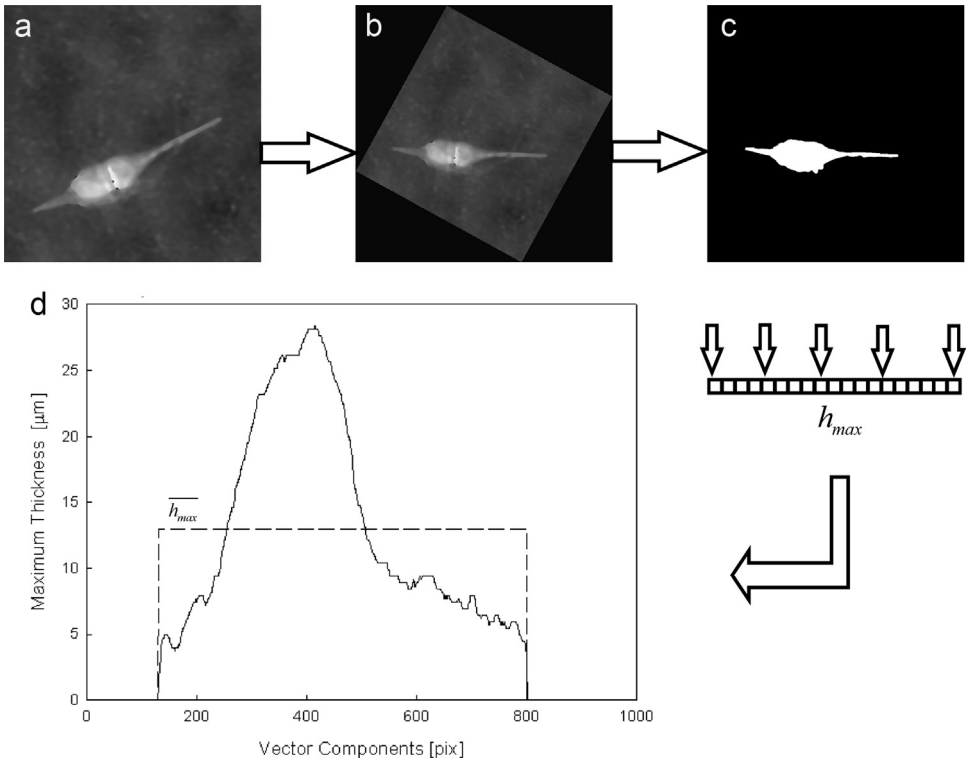

Fig. 4. Thickness calculation procedure. (a) Phase contrast image of a *C. Hirundinella* in dorsoventral position (as they appear in a microscope field), (b) rotated image, (c) binarized image and (d) solid line: thickness profile (h_{max}); dotted line: average of maximum thicknesses ($\overline{h_{max}}$).

processing procedures designed "*ad hoc*", using an appropiate threshold [30] and the application of several morphological operations, such us "erosion" and "dilation".

It is worth noting that, as many biological specimens, *C. Hirundinella* appears essentially transparent under bright field microscopy, making it difficult to extract the 2D ROI. Therefore, phase images are chosen over amplitude ones since they are more suitable for segmentation procedures [31].

From the binarized image, the automatic calculation of the maximum thickness profile is achieved by generating a row vector, whose components are obtained by adding all values of each column in the image. Background pixels do not contribute to the sum because they are zero valued, while those inside the cell take the value 1. Thus, the components of the generated row vector contain the values of the thickness in pixel units. The maximum thickness profile$h_{\max}$, which is plotted in Fig. 4(d), is determined by multiplying the row vector by the image factor scale, i.e. the unit of length that each pixel represents depending on the microscope objective used.

From the cell in frontal position, the phase map of Fig. 3(d) is rotated until the cell is layed down along the longitudinal axis. Then, a row vector, whose components contain the maximum phase delays for each column is generated. As an example, a typical maximum phase delays vector $\phi_{\max}$is plotted in Fig. 5.

Even though it is not necessarily true that the maximum thickness profile $h_{\max}$ is tied to the maximum phase delays $\phi_{\max}$, on average, a certain correlation may be expected, as long as the cell has a constant *effective refractive index* $\bar{n}$. Therefore, our hypothesis is put forward in terms of averages; both quantities, $h_{\max}$and $\phi_{\max}$, are averaged (dotted lines in Figs. 4 and 5), so that the average of maximum thicknesses $\overline{h_{\max}}$ corresponds to an equivalent phase delay $\overline{\phi_{\max}}$. This assumption implies averaging the cell shape in order to adopt an equivalent parallelepiped shape. Each cell $\Delta\bar{n}$ can be obtained from Eq. (2) resulting:

$$\Delta\bar{n} = \frac{\lambda}{2\pi}\frac{\overline{\phi_{\max}}}{\overline{h_{\max}}} \tag{5}$$

Replacing Eq. (5) in Eq. (4), the biovolume can be estimated by

$$V = \frac{\overline{h_{\max}}}{\overline{\phi_{\max}}}\sum \phi(i,j)\Delta x\Delta y \tag{6}$$

Eq. (6) shows that biovolume, as a global quantity, can be easily estimated with a hybrid methodology which combines phase delays introduced by the cell with a geometrical measure regarding to maximum thicknesses; this is accomplished without prior knowledge of intracellular refractive index. However, this calculation requires the cell to roll, either by gently tapping the cover slip with a pin-like object or by using external devices. Instead, taking advantage of *C. Hirundinella* size uniformity and exploiting the fact that they naturally appear in dorsoventral position, we propose to avoid cell manipulation, using a representative maximum thickness H calculated from the average silhouette of different individuals. Hence, Eq. (6) is modified resulting in:

$$V = \frac{H}{\overline{\phi_{\max}}}\sum \phi(i,j)\Delta x\Delta y \tag{7}$$

Although Eq. (7) suggests that cells adopt a shape proportional to the optical phase map, which is not the real cell morphology, accurate biovolume estimations are expected.

If machine vision is the ultimate goal, this would facilitate the automatization process, since for each sample, the average thickness could be extracted automatically without needing single cell rotation.

3. Results and discussion

To validate the size uniformity hypothesis, measurements on images from bright field microscope, for twenty randomly selected specimens, were performed, resulting in a maximum length of (171 ± 2) μm, a maximum width of (44 ± 1) μm and a body thickness of (25.4 ± 0.5) μm with coefficients of variation of 5%, 7% and 4% respectively. The low coefficient variation in the body thickness supports the use of the average value H in Eq. (7).

Following the proposed methodology, 21 *C. Hirundinella* holograms were recorded and their individual biovolumes were calculated using Eq. (7); obtained values are shown as fill dot in Fig. 6. For this task, phase maps, as shown in Fig. 3(d), were multiplied by a binary mask guaranteeing that only cell phase values were added up. For comparison purposes, values calculated using geometric approximations, following the same methodologies proposed by Vadrucci et al. [8] and Sun et al. [9], are also included. These calculations were carried out following the most frequent used *Ceratium* genus form consisting of an ellipsoid for the body, two cones for the antapical horns and a cylinder for the apical horn.

As it can be seen, biovolume calculated by the proposed methodology exhibits minor data dispersion than those obtained

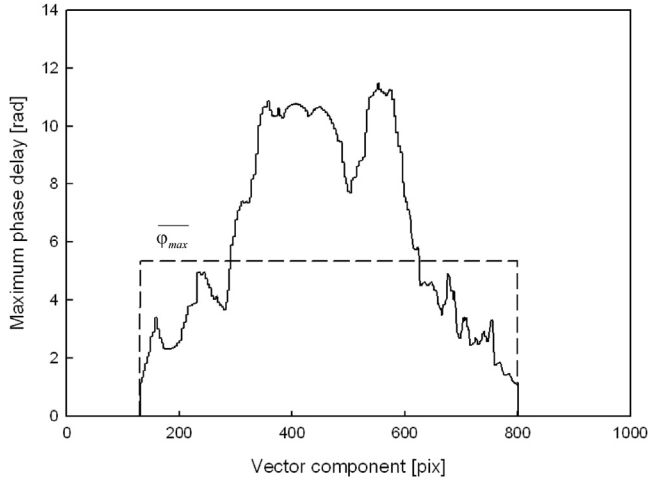

Fig. 5. Solid line: Maximun phase delay profile ($\phi_{\max}$). Dotted line: equivalent phase delay ($\overline{\phi_{\max}}$).

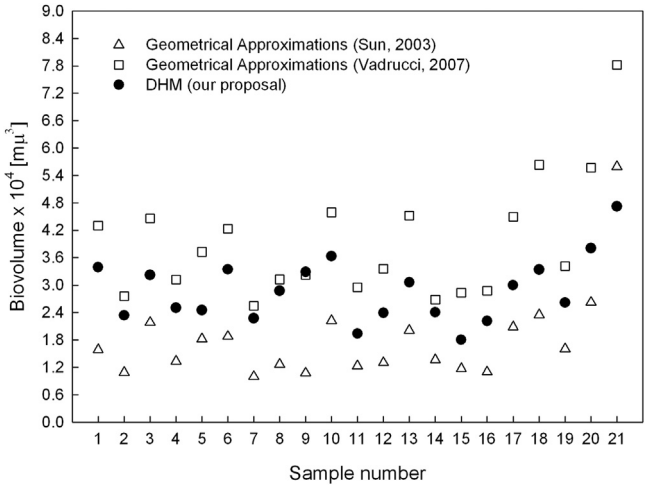

Fig. 6. Biovolume data for *C. Hirundinella*.

Table 1
Estimated average biovolume for *C. Hirundinella*

	Sun et al. [9]	Vadrucci et al. [8]	DHM
Average biovolume $\times 10^4$ [μm^3]	(1.8 ± 2.2)	(3.9 ± 2.8)	(2.9 ± 1.4)
CV* (%)	55	33	24

* Coefficient of variation.

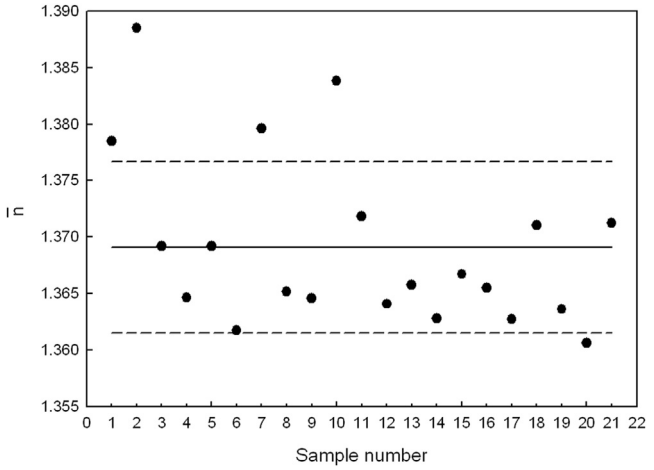

Fig. 7. Individual value of $\bar{n}$ for each *C. Hirundinella*. Solid line represents mean $\bar{n}$value and dashed lines $\bar{n} \pm \sigma$.

by geometrical approximations. Comparative statistical analysis is summarized in Table 1.

Even though Sun et al. and Vadrucci et al. calculate cell biovolume using the same geometrical model, they differ in the assumptions made for measuring the hidden dimension, which explains the quite different values aroused from the calculation. On the other hand, geometrical methods demand the measurement of at least six linear dimensions, increasing errors in volume estimation. According to Eq. (7), our hybrid methodology also requires the measurement of the linear dimension H, but a more representative quantity of the sample overall is expected due to it arises from an averaging process.

By making a more detailed analysis of the potential usefulness of Eq. (7), it can be seen that biovolume is proportional to the discretized integral of the optical phase. Physically, it represents the nonaqueous water content of the cell, which can be converted appropriately in the cell "dry mass" provided that the refractive index is known [32]. In this sense, our approach allows the calculation of an *effective refractive index* $\bar{n}$ for each individual studied using Eq. (5) and a measurement of the surrounding media refractive index n_0. Results for $\bar{n}$ are plotted in Fig. 7.

For the sample under study, n_0 measured with an Abbe refractometer yields $n_0 = 1.3345 \pm 0.0005$ corresponding to a wavelength of 632.8 nm. To support our hypothesis, $\bar{n}$ values obtained are in good agreement with reported ones for phytoplankton. Moreover, the mean value, $\bar{n}_{average} = 1.369 \pm 0.004$, falls within the expected value range for dinoflagellates [29].

It is interesting to note that the outliers in Fig. 7 have biovolume within normal range in Fig. 6. In this sense, these cells might actually have an intracellular refractive index higher than the average, or the deviations observed could proceed from the hybrid methodology nature, which could be a consequence from the assumptions made when deriving Eq. (7).

One particular aspect to consider is the criterium for deciding if the cells are in the positions required by our methodology. On this point, specialist expertise plays an important role. The cell was considered in dorsoventral position when only one antapical horn was displayed in the silhouette and any deviation from the real position was minimized by taking the average of a series of values. Concerning the frontal position choice, the most accurate value achieved was an approximate estimation based on the expert specialist's skills. It is worth remarking that this is not only an inherent matter of the proposed method but also of the geometrical models. Nonetheless, small deviations from frontal position may not be crucial for the present results since a compromise between accuracy and practicality of the determination is necessary to minimize the effort of linear microscopic measurements.

4. Conclusions

Digital Holographic Microscopy is proposed as an alternative for cell biovolume measurements. Particularly, in the case of *Ceratium* genus the rare and quite variable shape of the cell require complicated equations for biovolume calculations by geometrical approximations. A typical model is composed of different geometric shapes, requiring several length and diameter measurements per cell, and even with this time-consuming procedure, the biovolume cannot be adequately calculated. Particularly, the flattening of the cell and the ventral side excavation cannot be measured in fixed samples, and several assumptions have to be made. Nonetheless, this is not an issue for the proposed method as it takes into account, disregarding of *C. Hirundinella* 3D shape, the phase delays which depends on morphology and cell refractive index. Thus, biovolume is computed considering not only its geometrical volume, but also its intracellular content. From these considerations it can be concluded that this method could provide a more representative measurement as a biomass descriptor. The proposed methodology could be extended to the measurement of any species biovolume as long as they can be found easily in dorsoventral position and a uniform size distribution can be verified.

Acknowledgments

The authors acknowledge the valuable collaboration of Miss F. Ardaya in reviewing the English writing. This work was supported by ANPCyT-PME 1392/2 and Research Council of the National University of Salta, Project no. 1888.

References

[1] J. Gao, J.A. Lyon, D.P. Szeto, J. Chen, In *vivo* imaging and quantitative analysis of zebrasfish embryos by digital holographic microscopy, Biomed. Opt. Express 3 (2012) 2623–2635.
[2] B. Javidi, S. Yeom, I. Moon, M. Daneshpanah, Real-time automated 3D sensing, detection, and recognition of dynamic biological micro-organic events, Opt. Express 14 (2005) 3806–3929.
[3] J. Alvarez-Borrego, R. Mouriño-Pérez, G. Cristóbal, J.L. Pech-Pacheco, Invariant recognition of polychromatic images of *Vibrio Cholerae* O1, Opt. Eng. 41 (2002) 827–833.
[4] E. Alanis., G. Romero, L. Alvarez, C. Martinez, M.A. Basombrio, Optical detection of Trypanosoma-Cruzi in blood samples, for diagnosis purpose, Proc. SPIE 5622 (2004) 24–28.
[5] J.L. Pech-Pacheco, J. Alvarez-Borrego, Optical-digital system applied to the identification of five phytoplankton species, Mar. Biol. 132 (1998) 357–365.
[6] G.G. Romero, A.C. Monaldi, E.E. Alanís, Digital holographic microscopy for detection of Trypanosoma-Cruzi parasites in fresh blood mounts, Opt. Commun. 285 (2012) 1613–1618.
[7] B.I. Konoplya, F.S. Soares, New geometric models for calculation of microalgal biovolume, Braz. Arch. Biol. Technol. 54 (2011) 527–534.
[8] M.R. Vadrucci, M. Cabrini, A. Basset, Biovolume determination of phytoplankton guilds in transitional water ecosystems of mediterranean ecoregion, Transit. Waters Bull. TWB 2 (2007) 83–102.
[9] J. Sun, D. Liu, Geometric models for calculating cell biovolume and surface area for phytoplankton, J. Plankton Res. 25 (2003) 1331–1346.

[10] H. Hillebrand, C. Dieter Dürselen, D. Kirschtel, U. Pollingher, T. Zohary, Biovolume calculation for pelagic and benthic microalgae, J. Phycol. 35 (1999) 403–424.
[11] U. Schnars, W.O. Jueptner, Digital holography, Digital Hologram Recording, Numerical Reconstruction and Related Techniques, Springer-Verlag, Berlin Heidelberg, Germany, 2005.
[12] E. Cuche, P. Marquet, C. Depeursinge, Simultaneous amplitude-contrast and quantitative phase-contrast microscopy by numerical reconstruction of Fresnel off-axis holograms, Appl. Opt. 38 (1999) 6994–7001.
[13] B. Rappaz, P. Marquet, E. Cuche, Y. Emery, C. Depeursinge, P.J. Magistretti, Measurement of the integral refractive index and dynamic cell morphometry of living cells with digital holographic microscopy, Opt. Express 13 (2005) 9361–9373.
[14] I. Moon, B. Javidi, Shape tolerant three-dimensional recognition of biological microorganisms using Digital Holography, Opt. Express 13 (2005) 9612–9622.
[15] F. Charière, N. Pavillion, T. Colomb, C. Depeursinge, T.J. Heger, E.A.D. Mitchell, P. Marquet, B. Rapaz, Living specimen tomography by digital holographic microscopy: morphometry of testate amoeba, Opt. Express 14 (2006) 7005–7013.
[16] F. Palacios, J. Ricardo, D. Palacios, E. Gonçalves, J.L. Valin, R. De Souza, 3D image reconstruction of transparent microscopic object using digital holography, Opt. Commun. 248 (2005) 41–50.
[17] F. Charrière, A. Marian, F. Montfort, J. Kuehn, T. Colomb, T.J. Hegera, E.A. D. Mitchella, P. Marquet, C. Depeursinge, Cell refractive index tomography by digital holographic microscopy, Opt. Lett. 31 (2005) 178–180.
[18] F. Merola, L. Miccio, P. Memmolo, G. Di Caprio, A. Galli, R. Puglisi, D. Balduzzi, G. Coppola, P. Netti, P. Ferraro, Digital holography as a method for 3D imaging and estimating the biovolume of motile cells, Lab Chip 13 (2013) 4512–4516.
[19] G.N. Vishnyakov, G.G. Levin, Optical microtomography of phase objects, Opt. Spectrosc. 85 (1998) 73–77.
[20] M. Kim, Tomographic three-dimensional imaging of a biological specimen using wavelength-scanning digital interference holography, Opt. Express 7 (2000) 305–310.
[21] L. Yu, M. Kim, Wavelength-scanning digital interference holography for tomography three-dimensional by use of the angular spectrum method, Opt. Lett. 30 (2005) 2092–2094.
[22] R.F. Van Ligten, H. Osterberg, Holographic Microscopy, Nature 211 (1966) 282–283.
[23] D.C. Ghiglia, M.D. Pritt, Two dimensional Phase Unwrapping, Theory Algorithms and Software, John Wiley & Sons, New York, 1998.
[24] A. Baldi, F. Bertolino, F. Ginesu, On the performance of some unwrapping algorithms, Opt. Laser Eng. 37 (2002) 313–330.
[25] X. Su, W. Chen, Reliability-guided phase unwrapping algorithm: a review, Opt. Lasers Eng. 42 (2004) 245–261.
[26] E. Zappa, G. Busca, Comparison of eight unwrapping algorithms applied to Fourier transform profilometry, Opt. Lasers Eng. 46 (2008) 106–116.
[27] T.J. Flynn, Consistent 2-D phase unwrapping guided by a quality map, in: Proceedings of the 1996 International Geoscience and Remote Sensing Symposium, Lincoln, NE, 1996, pp. 2057–2059.
[28] R.E. Green, H.M. Sosik, R.J. Olson, M.D. DuRand, Flow cytometric determination of size and complex refractive index for marine particles: comparison with independent and bulk estimates, Appl. Opt. 42 (2003) 526–541.
[29] E. Aas, Refractive index of phytoplankton derived from its metabolite composition, J. Plankton Res. 18 (1996) 2223–2249.
[30] N. Otsu, A threshold selection method from gray level histograms, IEEE Trans. Syst. Man Cybern. 9 (1979) 62–66.
[31] P. Memmolo, G. Di Caprio, C. Distante, M. Paturzo, R. Puglisi, D. Balduzzi, A. Galli, G. Coppola, P. Ferraro, Identification of bovine sperm head for morphometry analysis in quantitative phase-contrast holographic microscopy, Opt. Express 19 (2011) 23215–23226.
[32] G. Popescu, Y.K. Park, N. Lue, C. Best-Popescu, L. Deflores, R.R. Dasari, M.S. Feld, K. Badizadegan, Optical imaging of cell mass and growth dynamics, Am. J. Physiol. Cell Physiol. 295 (2008) C358–C544.